Computing Curvature by Quadratic Approximation for Steep Dips

Marcos Machado, Petrobras
Marcelo Gattass, PUC-Rio
Ana Moliterno, Petrobras
Adelson de Oliveira, Petrobras

This paper was prepared for presentation during the 13th International Congress of the Brazilian Geophysical Society held in Rio de Janeiro, Brazil, August 26-29, 2013.

Abstract

Curvature is widely used in seismic interpretation. One of the most common approaches for computing volumetric curvatures is based on fitting of a simple quadratic surface for each point of the volume. The curvature attributes are subsequently obtained from the coefficients of this surface. This paper discusses this approach and proposes an adaptive rotation of axes to improve its performance for steep dips. A modification of the traditional algorithm is proposed, and tests with synthetic and real data are presented.

Introduction

Curvature attributes are widely used in seismic interpretation to image folds and flexures, sub-seismic antithetic faults that appear as drag or folds adjacent to faults, diagenetically altered fractures, karst, and differential compaction over channels (Marfurt *et al.*, 2010).

Initially, curvature was computed only from interpreted horizons. In the method proposed by Roberts (2001), a least squares quadratic surface is fitted to each horizon point, using the surrounding eight grid values. The curvature attributes are subsequently obtained from the quadratic surface.

Currently, the curvature can be evaluated directly from 3D seismic data. Two basic approaches exist to compute volumetric curvature, and both use a previously computed dip volume. In the first approach, a quadratic surface is built for each point of the volume. The surface is defined as an explicit function $z = f(x, y)$ from which the curvature can be evaluated. The coefficients can be computed by the least-squares method (Klein et al., 2008) or directly from the dip volume (Al Dossary *et al.,* 2006, Rich, 2008). The second approach is based on the implicit function representation of the structures present on the data volume (Donias *et al.*, 1998, Martins *et al.*, 2012).

This paper aims to analyze and improve the behavior of the curvature attributes computed via quadratic approximation in the presence of high dip values. A modification of the traditional algorithm is proposed, and tests with synthetic and real data are presented.

Computing Curvature by Quadratic Approximation

One concept used to describe the geometry of a reflector present in 3D seismic data addresses its orientation. The reflector can be viewed as a piecewise continuous surface, and each point of the surface has a tangent plane defined by its normal vector **n**. The tangent plane describes the neighborhood near that point of the structure in terms of its orientation. Given the normal vector

$$\mathbf{n}^T = (n_z, n_x, n_y), \quad (1)$$

where z is the vertical coordinate (time or depth), x and y are the spatial coordinates and with n_z chosen as semi-positive ($n_z \geq 0$), we can identify the dip and azimuth. If we let p and q be the components of the dip in the directions X and Y, respectively, it is possible to show that

$$p = \frac{-n_x}{n_z} \quad (2)$$

$$q = \frac{-n_y}{n_z} \quad (3)$$

Another useful concept for describing the geometry of a structure is the curvature. Curvature is a geometric measure of how the surface bends. Using the normal vectors, it describes how the normal vectors change in the neighborhood of each point.

While the orientation of a given point in a seismic horizon can be fully described by its tangent plane, local variations of the normal to the horizon can be accommodated in an imaginary quadratic surface. The approach based on quadratic surface approximation for curvature computation of a seismic horizon was presented by Roberts (2001). Following his notation, we consider a surface described as single-value function

$$z(x,y) = ax^2 + by^2 + cxy + dx + ey + f \quad (4)$$

The point at which the curvature will be computed corresponds to $x = 0$ and $y = 0$.

Al Dossary *et al*. (2006) proposed an automatic computation of the coefficients of the z function from the previously computed dip volume. The two dip components p and q are related to the z function at point (0, 0) by:

$$p = \frac{\partial z}{\partial x} \quad (5)$$

$$q = \frac{\partial z}{\partial y} \quad (6)$$

Therefore, differentiating (4) and using (5) and (6), the coefficients can be obtained as shown:

$$\frac{\partial}{\partial x}\frac{\partial z}{\partial x} = 2a = \frac{\partial p}{\partial x} \quad (7)$$

$$\frac{\partial}{\partial y}\frac{\partial z}{\partial y} = 2b = \frac{\partial q}{\partial y} \quad (8)$$

$$\frac{\partial q}{\partial x} + \frac{\partial p}{\partial y} = 2c \quad (9)$$

$$d = p \quad (10)$$

$$e = q \quad (11)$$

Once the set of coefficients is computed, we can obtain the various types of curvature, e.g., the mean and Gaussian curvature can be calculated as in Roberts (2001):

$$k_{mean} = \frac{a(1+e^2) + b(1+d^2) - cde}{(1+d^2+e^2)^{3/2}} \quad (12)$$

$$k_{Gauss} = \frac{4ab - c^2}{(1+d^2+e^2)^2} \quad (13)$$

Testing the Quadratic Approximation *z=f(x, y)*

In this paper, we tested the quality of the quadratic approximation with a spherical shell. A sphere with radius R has a constant curvature equal to 1/R. We built a synthetic volume containing a single spherical shell with a radius equal to 50 samples. To avoid sampling problems, the shell was built using a thickness of 7 samples; the central sample has an amplitude value of 1.0 and the other 6 values are such that the shell presents a radial cubic decay from the central sample.

The dip was computed using the gradient approach. We chose the spherical data as the input for the Gaussian derivative operator (with standard deviation equal to 1.0) and applied the structure tensor (Bakker, 2002) as a smooth vector filter with Gaussian weights (standard deviation equal to 2.0). The dip obtained was qualitatively satisfactory, as shown in Figure 1 (dark green color corresponds to -45° and blue to less than -67° values). This figure presents the dip crossline component mapped on a spherical surface with a radius of 50 extracted from the synthetic volume.

We would use the dip values obtained directly from the sphere construction method; however, the two set of values are very similar and this change didn't produce important difference for curvature values.

Computing the mean curvature for these data, we observe that the values are close to the expected value of 0.02, at least until near 30°. However, these values tend to decrease as the angle increases. This behavior can be observed in Figure 2 in which we present the graph for the mean curvature plotted against the dip angle for a constant azimuth (along the *y* = 0 plane).

The same behavior can be observed in Figure 3 in which the mean curvature was mapped on the same surface of Figure 1. In Figure 3, blue corresponds to 0.020, green to 0.015, yellow to 0.014 and red to values less than 0.012.

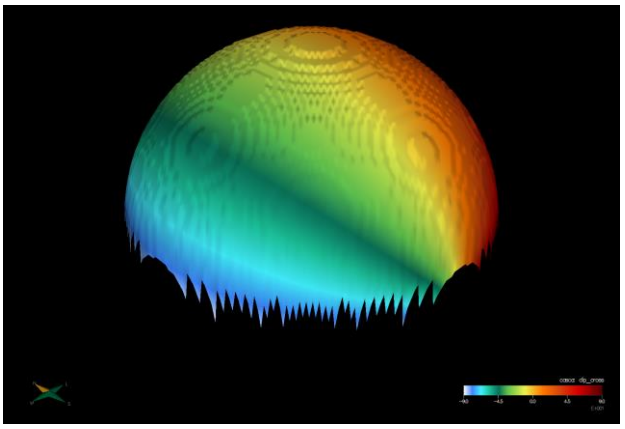

Figure 1: Dip crossline component mapped on the spherical shell.

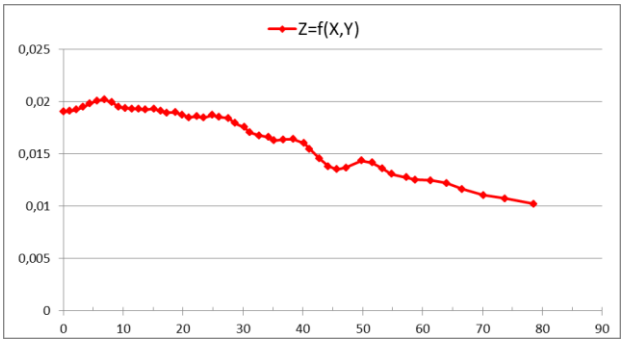

Figure 2: Graph of the mean curvature plotted against angle for the spherical shell.

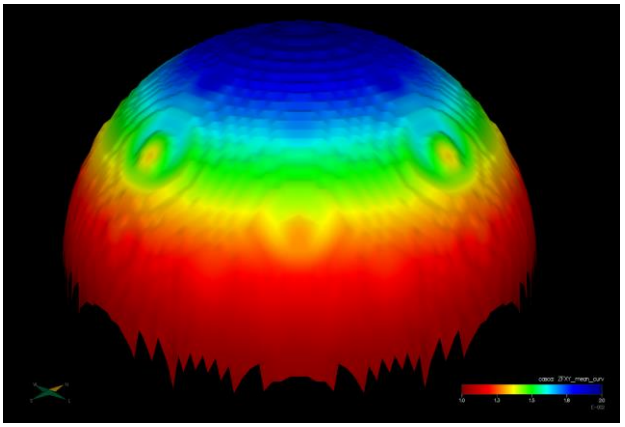

Figure 3: Mean curvature computed with *z=f*(*x*, *y*) approximation mapped on the spherical shell.

The problem is numeric. For small dip, both the first derivatives of z (d and e), present in the denominator of expressions (12) and (13), and the second derivatives of z (a, b and c), present in the numerator, assume small values. As the dip angle increases, both numerator and denominator also increase. In particular, for 90^o, they go to infinity. Mathematically, for an ideal sphere, they change with an equal rate in such a way that it keeps constant the curvature value. However, for discrete sphere data the computation results unstable and, in our test, the curvature decreases with dip.

Combining three Quadratic Approximations: $z=f(x, y)$, $x=f(y, z)$ and $y=f(z, x)$

To remedy the problem identified above, at least for angles greater than 45^o, we propose to use the quadratic approximation $z=f(x, y)$ from equation (4) only when the absolute value of the z component of the normal vector $|n_z|$ is the greatest in absolute value for the three components of $\boldsymbol{n}$. In other words, we use (4) only when $|n_z| \geq |n_x|$ and $|n_z| \geq |n_y|$. Otherwise, we change the roles of the three components by rotating the axes and rewriting equation (4).

If $|n_x| > |n_y|$ and $|n_x| > |n_z|$, we rotate -90° around the y axis. In this case, the old z axis becomes the new x axis, and the old x axis becomes the $-z$ axis. We apply these changes to equations (5) to (11). In this case, we build the quadratic approximation for $x = f(y, z)$.

If $|n_y| > |n_z|$) and $|n_y| > |n_x|$, we rotate -90° around the x axis. In this case, the old z axis becomes the -y axis, and the old y axis becomes the new z axis. In this case, we build the quadratic approximation for $y = f(z, x)$.

In Figure 4, we show the three regions determined by the normal components, as described previously, for the example of the spherical shell. The sphere is viewed from the top, and the blue color displays the points where we build the traditional approximation $z = f(x, y)$, whereas the white color displays the points where we build $x = f(y, z)$ and red denotes $y = f(z, x)$.

Observe that, while Al Dossary *et al*. (2006) approach has p and q as input for curvature computation, here, we need two components of the normal vector as input (the third one comes from the normalization). Again, this is important to avoid numerical problems.

Using this approach, we can compute the curvature and reduce the previously described numerical problems when the inclination of the surface is greater than 45°. Figures 5 and 6 show the improvement of the curvature computation in the proposed method compared with the classical proposal shown in Figures 2 and 3.

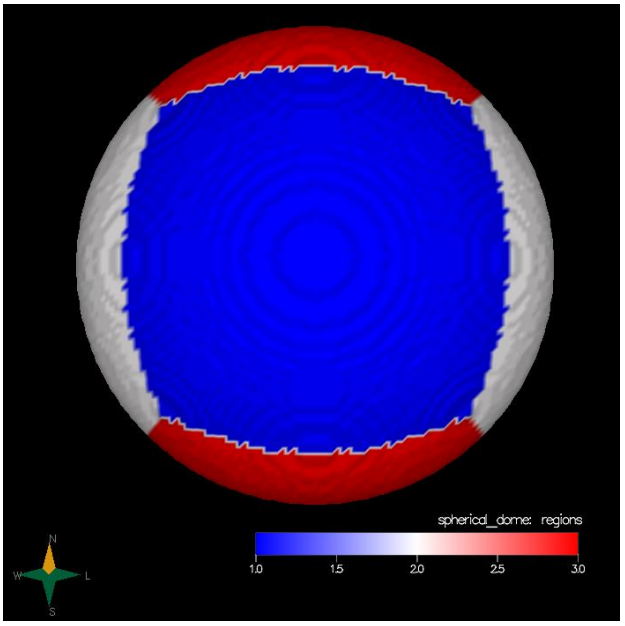

Figure 4: The three regions for the spherical shell.

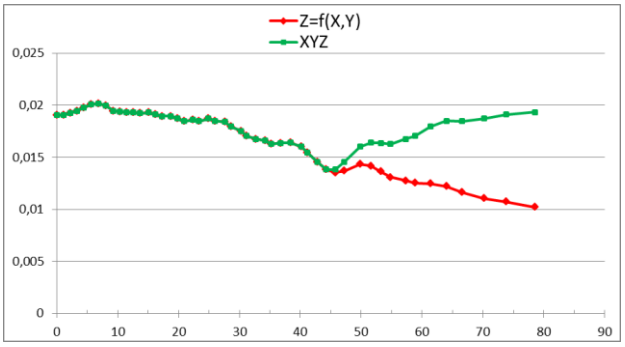

Figure 5: Graph of the mean curvature plotted against angle for the spherical shell with the two strategies. Red color corresponds to the traditional one and green color to the proposed one.

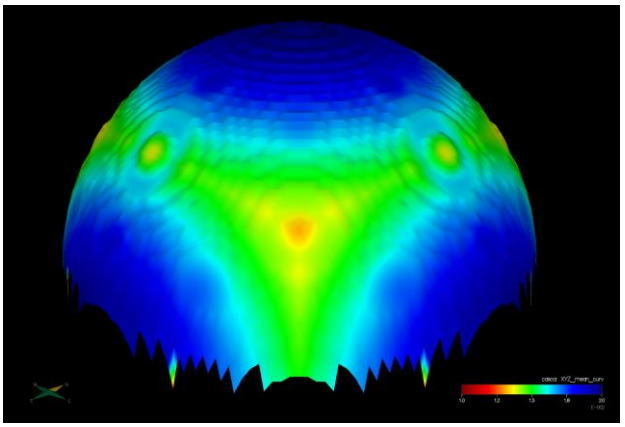

Figure 6: Mean curvature computed with $z=f(x, y)$ / $x=f(y, z)$ / $y=f(z, x)$ approximations mapped on a surface extracted from the sphere.

Algorithm

The proposed algorithm can be implemented as follows:

1. Compute the normal vector (n_z, n_x, n_y) for the input seismic volume.
2. For each point of the volume:
   2.1. If $|n_z| \geq |n_x|$ and $|n_z| \geq |n_y|$, then:
      2.1.1. $p = \frac{-n_x}{n_z}$; $q = \frac{-n_y}{n_z}$;

$$a = \frac{1}{2}\frac{\partial p}{\partial x};\ b = \frac{1}{2}\frac{\partial q}{\partial y};\ c = \frac{1}{2}\left(\frac{\partial q}{\partial x} + \frac{\partial p}{\partial y}\right)$$

   2.2. Else If $|n_x| > |n_y|$ and $|n_x| > |n_z|$, then:
      2.2.1. $p = \frac{n_z}{n_x}$; $q = \frac{-n_y}{n_x}$;

$$a = -\frac{1}{2}\frac{\partial p}{\partial z};\ b = \frac{1}{2}\frac{\partial q}{\partial y};\ c = \frac{1}{2}\left(-\frac{\partial q}{\partial z} + \frac{\partial p}{\partial y}\right)$$

      2.2.2. If $n_x < 0$, then:
         2.2.2.1. $p = -p;\ q = -q;$

$$a = -a;\ b = -b;\ c = -c$$

   2.3. Else If $|n_y| > |n_z|$ and $|n_y| > |n_x|$, then:
      2.3.1. $p = \frac{n_x}{n_y}$; $q = \frac{n_z}{n_y}$;

$$a = \frac{1}{2}\frac{\partial p}{\partial x};\ b = \frac{1}{2}\frac{\partial q}{\partial z};\ c = \frac{1}{2}\left(\frac{\partial q}{\partial x} + \frac{\partial p}{\partial z}\right)$$

      2.3.2. If $n_y > 0$, then:
         2.3.2.1. $p = -p;\ q = -q;$

$$a = -a;\ b = -b;\ c = -c$$

   2.4. $d = p;\ e = q;$
   2.5. Use a, b, c, d and e values to compute the desired curvature values for the current point as described in Roberts (2001) and Rich (2008).

The items 2.2.2.1 and 2.3.2.1 are necessary to adjust the approximations to the sign convention for the curvature attributes: positive for anticlines and negative for synclines.

Examples

We applied our algorithm to real 3D seismic data. The following images present snapshots for two vertical sections of the seismic amplitude. In Figure 7, an arrow marks the location of a fault, and this fault occurs in a region with a steep dip (see the horizontal slice in Figure 8). In Figure 9, we present the maximum curvature computed by the traditional algorithm; no curvature event appears to correspond to the fault. In Figure 10, however, we show the maximum curvature computed by our algorithm; observe the presence of an event of high curvature aligned with the fault.

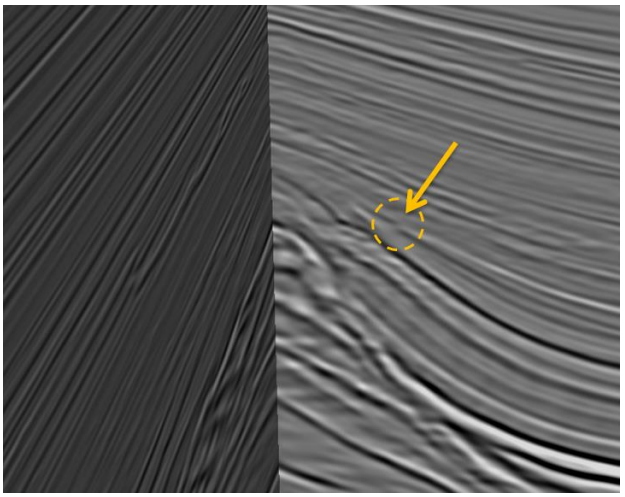

Figure 7: Two vertical sections showing a fault (denoted by the circle and the arrow).

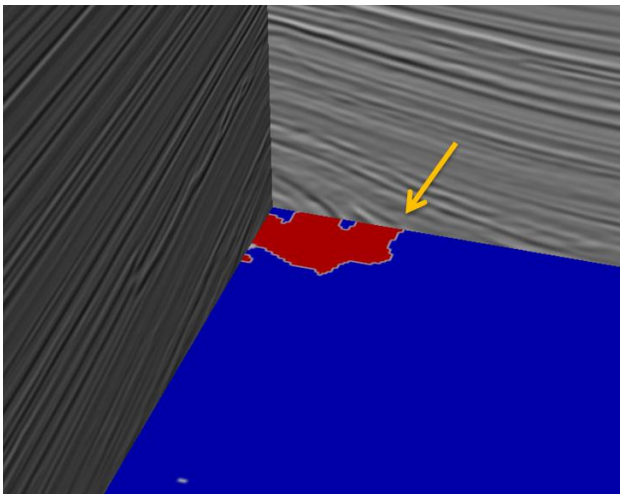

Figure 8: Time slice of the classes of the dips (same colors as in Figure 4).

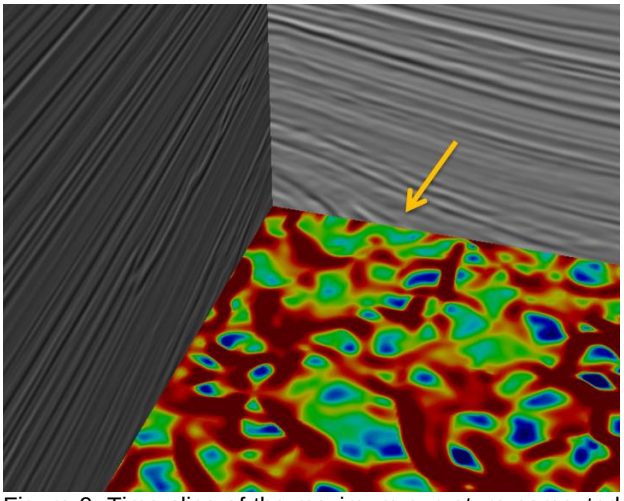

Figure 9: Time slice of the maximum curvature computed by the traditional algorithm.

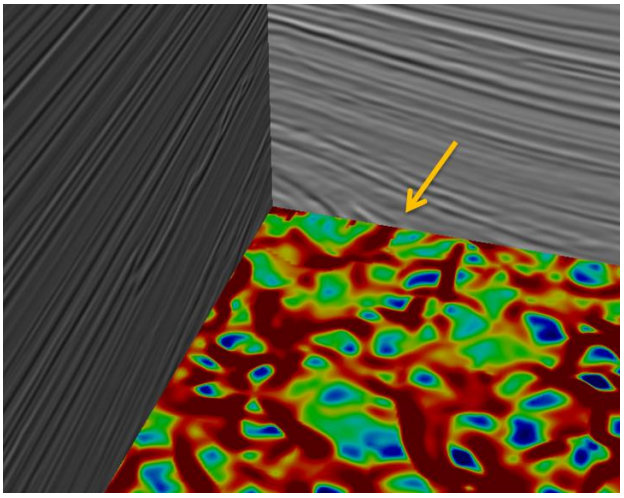

Figure 10: Time slice of the maximum curvature computed by the proposed algorithm. Note the curvature event aligned with the fault.

Conclusions

We tested the quality of curvature algorithms with a synthetic spherical shell. We verified that the traditional algorithm based on quadratic approximation produces poor performance for areas with steep dips. Next, we proposed an adaptive rotation of the axes to improve the performance. Using the new algorithm with real data, we showed that the obtained curvature is more compatible with the seismic data.

The proposed modification is quite simple to implement but treats only the situations of dips greater than 45°. Variations of our scheme can be developed to improve the curvature computation for structures with dip angles near 45°.

In general, the conditions necessary to apply the proposed rotations are not common in real data; normally, the reflectors are horizontal or show small dips. However, the 45° limit dip value refers to the dimensionless set of voxels, and therefore, this limit may correspond to a real angle value less than 45°.

Acknowledgments

We thank Petrobras for permission to publish this work. We also thank Alexandre Kolisnyk for helpful discussions.

References

Al Dossary, S., and K. J. Marfurt, 2006, 3D volumetric multispectral estimates of reflector curvature and rotation: Geophysics, 71, 41–51.

Bakker, P., 2002, Image structure analysis for seismic interpretation, PhD thesis, Delft University of Technology

Donias, M., P. Baylou and N. Keskes, 1998, Curvature of oriented patterns: 2-D and 3-D Estimation, from Differential Geometry, IEEE International Conference on Image Processing, 1, 236-40.

Marfurt, K. J., and J. Rich, 2010, Beyond curvature – volumetric estimates of reflector rotation and convergence, SEG, Expanded Abstracts

Martins, L. O., P. M. Silva and M. Gattass, 2012, A Method to Estimate Volumetric Curvature Attributes in 3D Seismic Data, 74th EAGE Conference

Rich, J., 2008, Expanding the applicability of curvature attributes through clarification of ambiguities in derivation and terminology, SEG, Expanded Abstracts

Roberts, A., 2001, Curvature attributes and their application to 3D interpreted horizons: First Break, 19, 85–100.